Hydrolysis of Evaporated Zn in a Hot Wall Flow Reactor

Tareq Abu Hamed
Jane H. Davidson
Mark Stolzenburg

Department of Mechanical Engineering,
University of Minnesota,
Minneapolis, MN 55455

Hydrolysis of Zn is investigated as the second step in a ZnO/Zn redox solar water splitting process. Zinc is evaporated and hydrolyzed with steam in a hot wall flow tubular reactor. The influence of the reactor temperature distribution and residence time on hydrogen conversion was measured for furnace set point temperatures of 1023 K and 1073 K. The yield of ZnO aerosol was measured in situ using a scanning differential mobility sizer. The composition and morphology of the solid product were characterized with X-ray diffraction and microscopy. Hydrogen conversions of 87–96% at temperatures above zinc saturation are attributed primarily to hydrolysis of zinc(g) at the wall of the reactor at temperatures from 800 K to 1077 K. [DOI: 10.1115/1.2969808]

Introduction

Hydrogen produced from water in solar driven thermochemical cycles is arguably one of the most promising options for long term storage of the world's most abundant energy source and for a carbon-free fuel. Direct thermolysis of water is not practical, but water splitting cycles based on metal redox reactions hold promise for practical implementation (reviewed in Refs. [1–6]). The focus of this study is the two-step zinc oxide/zinc redox cycle. The solar step is the endothermic dissociation of zinc oxide.

$$\mathrm{ZnO} \rightarrow \mathrm{Zn} + \tfrac{1}{2}\mathrm{O_2} \tag{1}$$

The dissociation chemistry and reactor technology are summarized in prior papers including Refs. [5,7–12]. At 2335 K, the Gibbs free energy for the dissociation reaction is zero and thus the endothermic reaction can be carried out using concentrated solar thermal energy without electricity input or carbothermal reduction. Thermal reduction of other metal oxides requires temperatures above those achievable in solar concentrating systems unless carbothermal or methanothermal reduction is used. The direct (without carbothermal reduction) solar dissociation of zinc oxide has been demonstrated in Switzerland and France [7–10,13,14]. Effective separation of the gaseous products is required to avoid reoxidation of Zn. The second step is the exothermic hydrolysis of Zn to produce hydrogen and ZnO.

$$\mathrm{Zn} + \mathrm{H_2O} \rightarrow \mathrm{ZnO} + \mathrm{H_2} \tag{2}$$

The product ZnO can be recycled in the solar reactor via reaction (1). The net reaction is the splitting of water. The fractional hydrogen conversion is defined as

$$\mathrm{H_2\ conversion} = \frac{\text{moles of } \mathrm{H_2}}{\text{moles of } \mathrm{H_{2,max}}} \tag{3}$$

where $\mathrm{H_{2,max}}$ refers to the theoretical maximum amount of $\mathrm{H_2}$ under complete hydrolysis of the Zn. The theoretical exergy efficiency of the cycle is 44% with complete heat recovery and 29% without any heat recovery [12].

The present study addresses the hydrolysis step (2). The desire is to produce $\mathrm{H_2}$ at high conversion and to recover ZnO for reprocessing in the solar step (1). The hydrolysis reaction is thermodynamically favorable at or below about 1490 K, but there are kinetic constraints. The prior studies most relevant to the present work are those that have measured hydrolysis of Zn powder in the absence of oxygen [15,16]. Other studies have been carried out with molten Zn [17,18].

Ernst [15] carried out a thermogravimetric analysis of hydrolysis of commercial zinc nanoparticles (164 ± 10 nm) at atmospheric pressure and water vapor mole concentrations of 0.1–0.5 in argon. At the initiation of the hydrolysis experiments, the particles were 95 percent Zn (by weight). The experiments focused on temperatures from 603 K to 633 K because very slow reaction rates were observed below 573 K and particle sintering occurred above 653 K. A fast surface reaction was followed by a slower diffusion limited reaction. The fast heterogeneous reaction rate was first order with respect to Zn and half order with respect to water vapor. The reaction rate followed an Arrhenius law with a pre-exponential constant of 2×10^{-5} mol/cm^2 s and an activation energy of 43 ± 7 kJ/mol. In the slower second regime, the reaction was independent of the water vapor fraction and the author attributed the limiting reaction step to diffusion of Zn ions within the ZnO lattice at the surface. In this diffusion limited reaction, the rate of reaction followed a parabolic law consistent with Wagner and Grunewald's [19] model for metallic oxidation. The measured activation energy of the diffusion process was identical to that measured for the fast reaction regime. The author attributed the low activation energy, relative to prior studies of oxidation of Zn, to the size of the particles, which affects the defect density at the metal/metal oxide interface and as a result the dissolution of Zn metal into the ZnO matrix. The impact of particle size on the rate of reaction is in agreement with the results of Park et al. [20] who found that the activation energy for oxidation of aluminum nanoparticles increases with decreasing particle size.

Vishnevetsky and Epstein [16] measured hydrolysis of zinc produced by the solar carbothermal reduction of ZnO powder (SOLZINC) to that of commercial zinc powder. The SOLZINC was produced using wood charcoal as the reducing agent. Prior to hydrolysis, the Zn powder contained 10–15% ZnO (by weight) and consisted of $2-7$ μm conglomerates of $200-500$ nanometer spherical particles. Batch hydrolysis was carried out in a packed bed at temperatures from approximately 458 K to 833 K at atmospheric pressure with a nitrogen carrier gas. Hydrolysis of the SOLZINC was compared to that of a commercial Zn powder at 791 K. The commercial powder was 98% purity and less than 10 μm in size. For both powders, at temperatures above 673 K, a fast surface reaction was followed by a slow diffusion limited reaction. For the SOLZINC, hydrogen yield during the fast reaction varied from 66% at 716 K to 81% at 833 K. The structure of the powder after hydrolysis was similar to that before hydrolysis for conversions as high as 75%. The authors suggest the reaction proceeded as water penetrated the spherical particles and reached the liquid Zn core. This model is in opposition to the model pro-

Contributed by the Solar Energy Engineering Division of ASME for publication in the JOURNAL OF SOLAR ENERGY ENGINEERING. Manuscript received August 9, 2007; final manuscript received December 13, 2007; published online September 8, 2008. Review conducted by Gilles Flamant. Paper presented at the 2007 ASME Solar Energy Division and Advanced Energy Systems Division Conference (ES2007), 2007, Long Beach, CA, June 27–29, 2007.

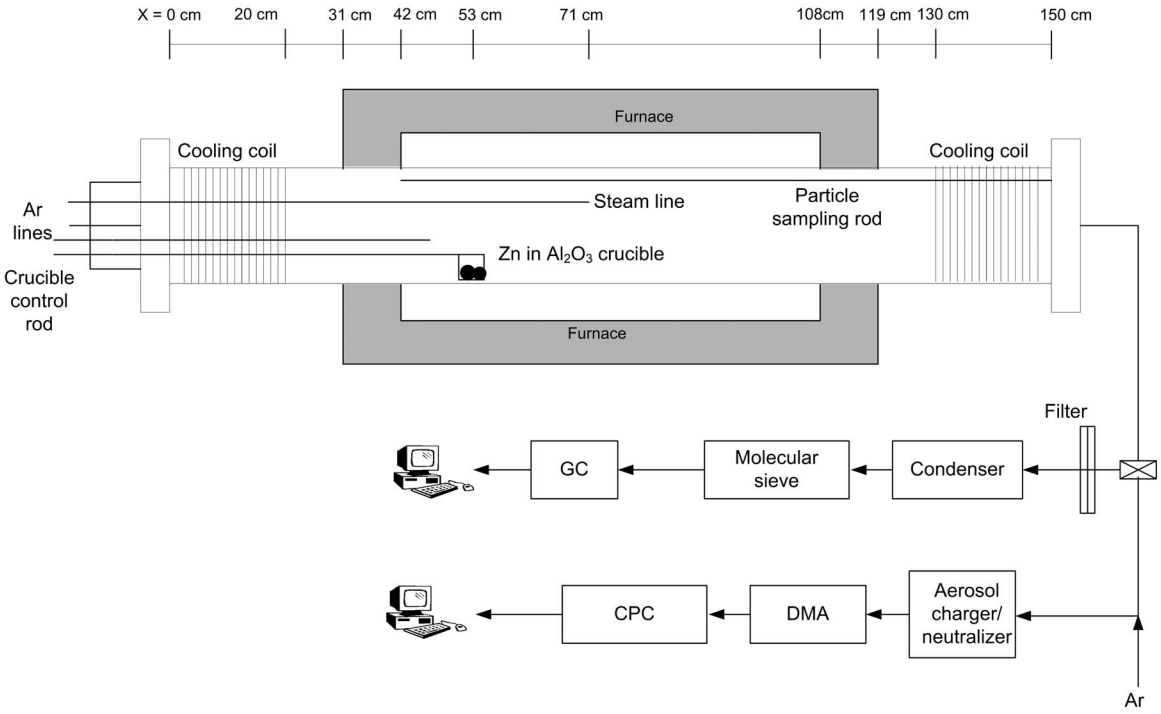

Fig. 1 The experimental apparatus

posed by Ernst [15] for lower temperatures as well as prior analysis of the oxidation of aluminum nanoparticles for which the transport of the molten aluminum to the outside of the particle was faster than the transport of the oxidizer though the oxide shell [21,22]. Notably, at 791 K, hydrogen conversion for the commercial Zn powder was approximately one-third that of the SOLZINC at 833 K. The difference in rates of conversion was attributed to differences in the powder size, consistent with the prior work.

In recognition of the enhanced reactivity of nanoparticles, researchers at ETH-Swiss Federal Institute of Technology [23,24] proposed cosynthesis of hydrogen and zinc oxide via simultaneous formation and hydrolysis of Zn nanoparticles. The intent is to create Zn nanoparticles in a condensation nucleation process with simultaneous hydrolysis. The potential advantages of using nanomaterials are their high specific surface area and large surface to volume ratio. Initial experiments were conducted in a hot wall tubular flow reactor. Evaporation of Zn was followed by in situ hydrolysis with steam in an argon carrier gas [23,24]. Hydrogen conversion was 72% with respect to the limiting reactant Zn at a reactor set point temperature of 1023 K and a residence time of 0.85 s. Hydrogen production was attributed to hydrolysis of Zn on the reactor walls and on a stainless steel rod that extended axially along the center of the reactor. Wall temperatures were not reported. Near the reactor inlet, where temperatures were above the saturation temperature of Zn, analysis of material scraped from these surfaces led to the conclusion that ZnO was formed by vapor deposition of Zn followed by hydrolysis. This process is undesirable as the product is difficult to recover. At downstream positions where the gas temperature was below the saturation temperature of Zn, both ZnO and Zn particles were present on the reactor surface. The authors inferred from the morphology of the deposit that heterogeneous hydrolysis followed deposition of Zn on the reactor surfaces. Material collected on a glass fiber filter positioned at the reactor exit was pure Zn. The mass of Zn capture by the filter was not reported.

In the most recent experiments reported by the group at ETH, a modified reactor was divided into three temperature zones in an attempt to separate the Zn evaporation, condensation, and hydrolysis steps [15,25] Experiments were conducted to determine the impact of gas temperature and the length of the condensation (cooling) zone on hydrogen conversion and particle characteristics. At gas temperatures above the Zn saturation temperature, hydrolysis occurred on the wall of the reactor producing hydrogen conversion of approximately 90%, but particle yield, based on the mass of material collected on a filter, was negligible. At gas temperatures below Zn saturation, hydrogen conversion decreased with decreasing reactor temperature. Total mass collected on a filter at the exit of the reactor remained very low. Only a small fraction of the hydrogen conversion can be attributed to hydrolysis of gas borne Zn particles. For example, at 573 K, the maximum hydrogen conversion from ZnO particles was only 13% based on reported particle mass and composition on the filter. Total H_2 conversion was 60%. The low total conversion was attributed in part to loss of Zn in the cooling zone upstream of the hydrolysis zone. At 850 K, the total H_2 conversion was 90% and maximum conversion attributable to particles was 17%.

The objective of this paper is to report the results of initial experiments conducted at the University of Minnesota in a hot wall flow reactor. The effects of the zinc evaporation temperature, carrier gas flow rate, and temperature along the length of the reactor on the hydrogen and zinc oxide production were investigated. Particle mass and size were measured in situ by sampling the gas flow. Composition and morphology of particles collected on a filter and from the walls of the reactor were analyzed using X-ray diffraction and transmission electron microscopy (TEM).

Apparatus and Experimental Method

A schematic of the reactor and instrumentation used to measure hydrogen concentration and particle size and mass at the reactor exit is provided in Fig. 1. The reactor is a 7 cm i.d., 152 cm long quartz tube placed in an 88 cm long concentric cylindrical electric

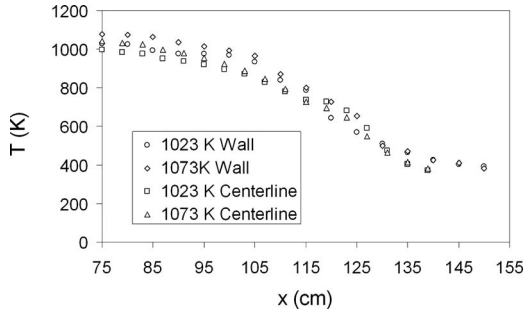

Fig. 2 The reaction zone wall and centerline temperature distributions. The furnace set point temperature is used as a reference to distinguish experiments.

furnace (Thermolyne 97500). Experiments were performed at furnace set point temperatures of 1023 K and 1073 K. A cooled inlet flange ($T=300$ K) contains ports in which argon carrier gas and steam were introduced. Products exited through a similar outlet flange ($T=390$ K). Zinc pellets (99.99% purity) of known weight were loaded in an alumina crucible positioned at $x=53$ cm ($T \approx 1000$ K), where $x=0$ is the position of the inlet. Ultrapure Ar was passed over the heated crucible to carry the evaporated Zn downstream and to prevent steam from entering the crucible. Argon was introduced via a 3.2 mm i.d. stainless steel tube supported at the inlet flange. The argon flow was measured with a mass flow controller (MKS Instruments). In the present study, experiments were conducted at Ar flow rates of 1750 ml/min and 2150 ml/min yielding residence times of 1.7 min and 2.1 min. These residence times are longer than those in earlier studies with a smaller diameter reactor tubes. Steam was generated by an electrical heater fed with de-ionized water by a peristaltic pump (Ismatec EW-78017). Steam was introduced in the reactor at 0.2 ml/min via a 3.2 mm i.d. stainless steel tube at $x=71$ cm. Axial mixing of the Zn and steam reduced backflow of the reactants. Products and the carrier gas leave the reactor through a 1.27 cm diameter stainless steel tube.

Prior to each experiment, the alumina crucible was loaded with 1 g of zinc and placed in the reactor. The reactor was evacuated to 25 mbars and purged with Ar. During a typical experimental run, the reactor was heated to the desired set point temperature without any gas flow to minimize evaporation during heat up. Approximately 5 min is required to heat up the furnace from 693 K (the zinc melting point) to furnace set point temperatures used in this study. Our observation is that very little zinc mass is evaporated during this time in comparison to the total experiment. In the visible portion of the quartz reactor tube at $x>119$ cm, condensation of zinc was not visible until the gas flows were initiated. Once the desired steady-state temperature was attained, the valves for the steam and the argon carrier gas were opened. The H_2O:Zn molar ratio was 50. Each experiment was continued until hydrogen concentration at the exit fell below the detectable limit (200 ppmv). The zinc was evaporated completely during a run. The centerline gas and wall temperature distributions in the reactor were measured using a chromel-alumel (*K*-type) thermocouple.

Measured temperatures are reported in Fig. 2 for the two furnace set point temperatures. Temperatures are those measured in the reactor from the furnace center to the reactor exit. The reference temperatures noted in the figure refer to the furnace set point temperature. Note that the gas and wall temperatures in both experiments are within 35–80 K of each other. Wall temperatures within the electrically heated zone within the furnace ($75 \le x \le 108$ cm) decreased from 1077 K to 966 K and from 1023 K to 933 K for furnace set point temperatures of 1073 K and 1023 K, respectively. Downstream the active heated zone at the insulation zone ($108 \le x \le 119$ cm), the wall temperatures decreased from 966 K to 728 K and from 933 K to 642 K for furnace set point temperatures of 1073 K and 1023 K, respectively. Temperature is maintained above 640 K for rapid hydrolysis. Downstream of the furnace at $119 \le x \le 130$ cm, the reactor temperatures decreased further. The wall temperatures in this zone decreased from 728 K to 499 K and from 643 K to 509 K for furnace set point temperatures of 1073 K and 1023 K, respectively. At these temperatures, significant hydrolysis was not expected. Further downstream at the cooled zone ($130 \le x \le 150$ cm), the wall temperatures drop slightly from 500 K to 390 K (at the filter) for both furnace set point temperatures.

To measure hydrogen concentration, the outlet gas stream was treated to remove moisture and any solid particles by passing it through a glass fiber filter, followed by a condenser and molecular sieve. The effluent hydrogen concentration was analyzed at 2 min intervals using an inline gas chromatograph (GC, Agilent 6890). The composition of material deposited on the quartz reactor surface and a rod inserted into the reactor was analyzed by X-ray diffraction (Bruker-AXS D5005 Diffractometer with 2.2 kW sealed Cu source). The particle morphology was observed using TEM with a FEI Tecnai T12 microscope with a resolution of 2 Å and Gatan Multiscan Camera at 120 kV.

The aerosol at the reactor exit was sampled in situ. Particle number concentration and size distribution were analyzed using a scanning differential mobility sizer (SMPS) [26]. This system consisted of a Po-210 radioactive aerosol charger/neutralizer, a nanodifferential mobility analyzer (DMA) (TSI 3085) with recirculating Ar sheath flow and an ultrafine condensation particle counter (CPC) (TSI 3025). Size distribution was measured in the range 3.1–71 nm where the size is the diameter of an equivalent sphere with the same mobility (or drag). Data were obtained every 23 s.

Table 1 Summary of operating conditions and results (H_2O: Zn molar ratio≈50)

No.	Set point T (K)	Q_{Ar} (ml/min)	Residence time (min)	Δt (min)	Q_{Zn} (10^{-4} mol/min)	T_{sat} (K)	H_2 Conversion (%)	Average H_2 Conversion (%)	Q_{H_2} (10^{-3} mol/min)
1	1023	1750	2.12	128	1.37	767	94	95	0.13
2				130			95		0.14
3	1023	2150	1.71	98	1.73	769	88	88	0.15
4				102			89		0.16
5	1073	1750	2.12	86	2.12	786	98	96	0.18
6				90			94		0.17
7	1073	2150	1.71	72	2.25	780	87	87	0.21
8				76			87		0.22

Results

Table 1 summarizes the operating conditions and results for eight experiments performed at furnace set point temperatures of 1023 K and 1073 K, and carrier gas flow rates of 1750 ml/min and 2150 ml/min. Experiments were performed in duplicate. Data reported in Table 1 include the average evaporation rate of Zn (Q_{Zn}), the Zn saturation temperature (T_{sat}), the hydrogen conversion (for each experiment and an average for duplicate experiments), and the hydrogen production rate (Q_{H_2}). The residence time and the duration of the experiment (Δt) are also listed. The flow of Zn is based on the initial mass of zinc and the duration of the experiment. This approach provides a reasonable estimate for experiments in which hydrogen production, temperature, and carrier gas flow rates are steady. It is justified by the close correlation of H_2 and Zn evaporation rates seen in prior work [23,25]. The zinc saturation temperature T_{sat} was calculated from [27]

$$\log P_{Zn,S} = -20.31 - \frac{4636.2}{T_{sat}} + 10.07 \log T_{sat} - 0.0038 T_{sat} + 4.89 \times 10^{-7} T_{sat}^{2} \quad (4)$$

where $P_{Zn,S}$ was determined from the mole fraction of the Zn using the evaporated mass of Zn and the measured mass flow rates of argon and steam. Hydrogen conversion was determined using Eq. (3) where the numerator is the sum of measurements of H_2 for the duration of each experiment. The denominator is based on the mass of evaporated zinc.

Hydrogen Production. Transient H_2 production (mol/min) is plotted for all experiments in Figs. 3(*a*)–3(*d*). Hydrogen conversion ranged from 87% to 98%. Repeatability was excellent. There is modest scatter in the data of Experiments 7 and 8 at a furnace set point temperature of 1073 K and an argon flow rate of 2150 ml/min. The highest H_2 conversion was achieved at the lower Ar flow rate of 1750 ml/min. Conversion is relatively insensitive to the change in furnace set point temperature from 1023 K to 1073 K. This result is expected for two reasons. First, we attribute hydrolysis to a heterogeneous reaction at the wall. Thus as will be discussed in the presentation of the XRD data, hydrolysis is more sensitive to local temperature near the wall than the furnace set point temperature. Second, the difference in furnace set point temperature is only 50 K and temperatures within the heated zone are above the saturation temperature of zinc. The slight increase in hydrogen conversion from 87–88% at 2150 ml/min to 95–96% at 1750 ml/min may be due to an increase in residence time (residence time is based on the length of the heated zone downstream of the position where steam is introduced, $71 \leq x \leq 150$ cm). Hydrogen production (Q_{H_2}) increased as the Ar flow rate and reactor temperature were increased due to the faster evaporation of the zinc. The measured hydrogen conversions are consistent with prior data obtained at temperatures above Zn saturation at ETH [25] and by Clarke and Fray [28] for oxidation of Zn by a mixture of H_2 and H_2O. Early experiments at ETH [23,24] produced lower hydrogen conversion perhaps due to shorter residence time (0.85 s) or differences in reactor surface temperature.

Product Zinc Oxide. The production of zinc oxide was examined by observation and analysis of deposits on the reactor wall as well as particles sampled in the effluent gas stream. In all experiments, deposits were observed on the wall of the quartz reactor for $31 \leq x \leq 150$ cm and along the sampling rod. The local wall temperature is the most important predictor of chemical composition and morphology of the deposit. In the heated reaction zone for $31 \leq x \leq 115$ cm where temperatures were above 800 K (800–1077 K), the deposit was attached tenaciously to the wall and was white to gray in color. Measured wall temperatures in this zone are above the saturation temperature of Zn except for the last few centimeters upstream of the exit. X-ray diffraction of material mechanically removed from the sampling rod showed that it was 100% ZnO (zincite), as indicated in Fig. 4(*a*). Representative TEM images of ZnO collected from the wall for Experiment 8 are shown in Fig. 5(*a*). A variety of morphologies and agglomerates are visible with sizes on the order of 50–100 nm. Because these deposits were formed at temperatures above Zn saturation, we

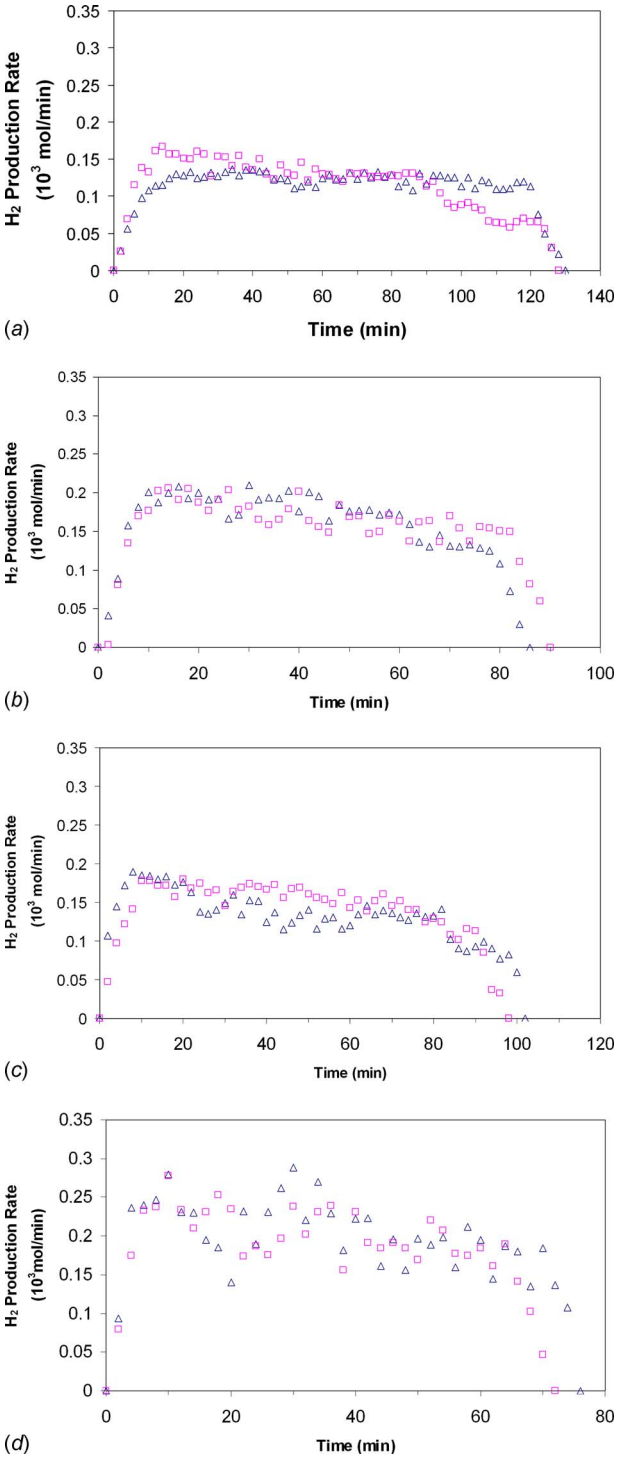

Fig. 3 H_2 production rate (*a*) 1023 K and 1750 ml/min Ar, (*b*) 1073 K and 1750 ml/min Ar, (*c*) 1023 K and 2150 ml/min Ar, and (*d*) 1073 K and 2150 ml/min Ar

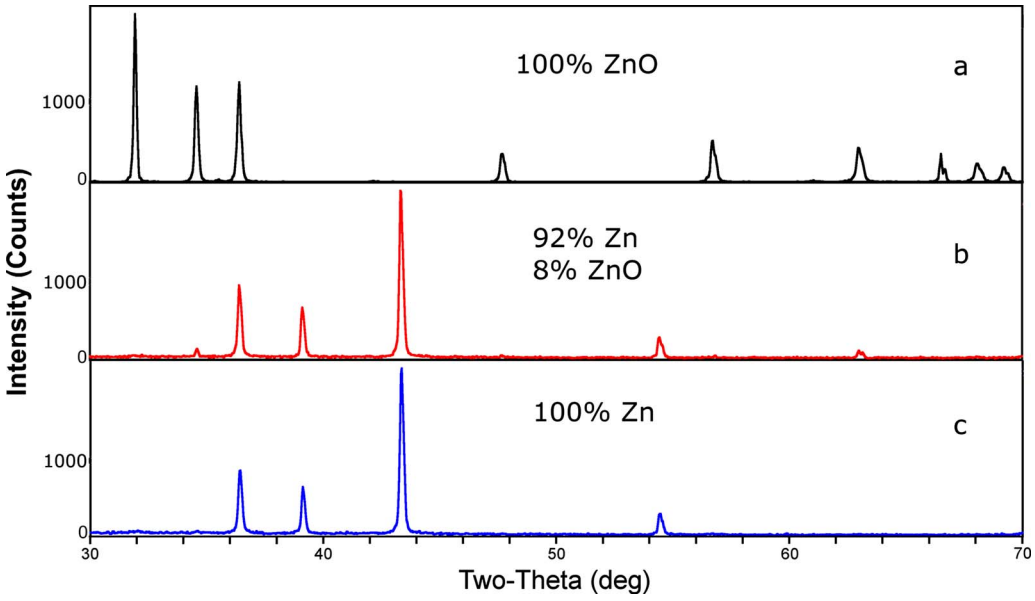

Fig. 4 XRD analysis of the particles collected in (*a*) the heated reaction zone for $31 \leq x \leq 115$ cm, (*b*) the cooler end of the reaction zone for $115 \leq x \leq 123$ cm, and (*c*) the quartz tube downstream of the heated reactor for $123 \leq x \leq 150$ cm

surmise the processes are vapor deposition and heterogeneous hydrolysis of Zn at the wall of the reactor. The difficulty in removing the deposit from the quartz tube provided additional support for a vapor deposition process. After cleaning, we did not observe etching of the quartz tube.

At the cooler end of the reaction zone at $115 \leq x \leq 123$ cm, where wall temperatures decreased from 800 K at $x = 115$ cm to 654 K at $x = 123$ cm, the material scraped from the reactor surface is 92% Zn and 8% ZnO (Fig. 4(*b*)). There was a gradual transition in color from white/gray to black. The amount

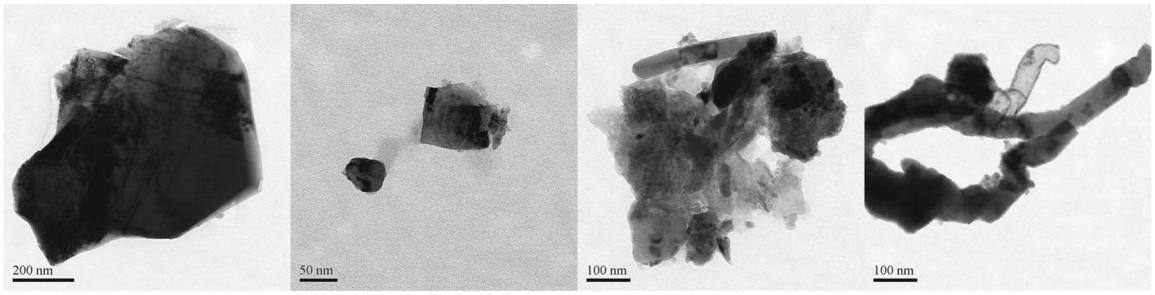

(a)

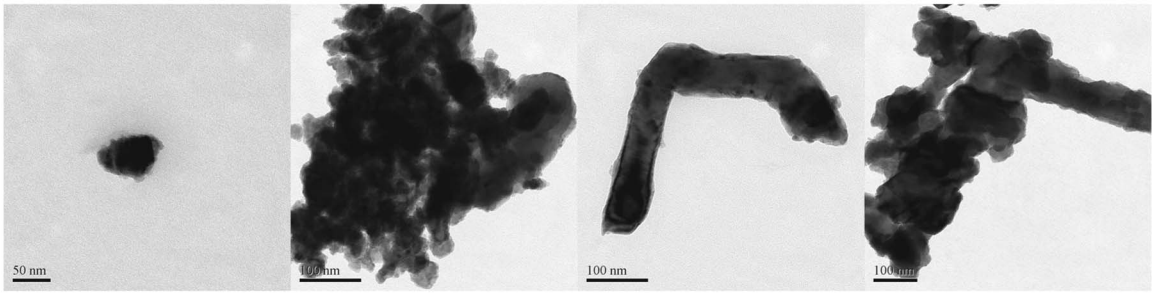

(b)

Fig. 5 TEM images of (*a*) ZnO and (*b*) Zn nanoparticles synthesized at 1073 K and 2150 ml/min. These particles were removed from the walls of the reactor.

of material on the wall increased with decreasing wall temperature. Based on observation of the deposit, the ZnO content is attributed primarily to the material deposited in the hotter region from $x=115$ cm to 117 cm. Material removed from the cooler region of this zone is most likely pure zinc. It is also possible that some of the deposited material underwent incomplete hydrolysis.

In the coolest section of the quartz tube well downstream of the heated reactor ($123 \leq x \leq 150$ cm) where wall temperatures dropped from 654 K to 382 K, all of the deposited material was black with a mirrorlike appearance. These deposits were easily removed with a brush and were 100% Zn (Fig. 4(*c*)). These results are consistent with the results reported by Ernst [15] in which hydrolysis of solid zinc nanoparticles was not measured for temperatures below 573 K. TEM images are shown in Fig. 5(*b*).

An aspirated probe was used to sample the gas stream in order to determine if aerosol particles were present. Data were obtained for a furnace set point of 1073 K and an Ar flow rate of 2150 ml/min. The aerosol distribution was bimodal with one mode centered just below 10 nm and the other at or above 70 nm. The size of the agglomerates and coalesced particles in the TEM images of Fig. 5(*a*) appears to be in the range of 50–100 nm corresponding to the upper mode of the measured bimodal airborne aerosol size distribution. This result suggests that the aerosol was formed in two stages. Aerosol may form by homogeneous nucleation of the hot zinc vapors when they enter the cooler zone of the reactor and again in the sampling tube where they cool further. The particles produced in the first stage would have more time to grow by condensation of zinc vapors and would constitute the larger of the two measured modes. A comparison of the molar production rates of H_2 and particles indicates that hydrogen production cannot be attributed to hydrolysis of aerosol. The rate for H_2 is on the order of 0.21×10^{-3} mol/min. If the particles are assumed to be ZnO, the rate for gas borne zinc oxide is only 12 nmol/min, which is far too low to account for the measured hydrogen production. It is possible that there is significantly more aerosol mass above the measurement range but it seems unlikely that it would account for the six orders of magnitude difference in the production rate of H_2 and ZnO.

Conclusion

We have built and operated a hot wall flow reactor for the in situ evaporation and hydrolysis of zinc in an argon carrier gas. Hydrogen production and the size and mass of the aerosol product were measured at furnace set point temperatures of 1023 K and 1073 K. Temperatures in the quartz reactor tube dropped from approximately 1000 K at the point where steam was introduced to 400 K at the exit. Residence time was varied from approximately 1.7 min to 2 min. The H_2O:Zn molar ratio was 50. The primary objective of these initial experiments was to better understand the mechanism of Zn hydrolysis.

Hydrogen conversion was 95–96% for a residence time of 2.1 min and 87–% for 1.7 min. Temperature played a crucial role in determining the extent of hydrolysis. Extensive deposition of ZnO was observed on the walls of the reactor in regions where the wall and gas temperatures were above 800 K. In cooler regions, the material deposited on the reactor wall was primarily zinc. The size distribution of aerosol at the reactor exit was bimodal with one mode at 10 nm and the other mode at or above 70 nm. Aerosol production was only 12 nmol/min, nearly six orders of magnitude too low to account for the measured hydrogen production. Thus we conclude that at these operating conditions, the probable mechanism for hydrolysis is vapor deposition followed by heterogeneous reaction on the wall of the hot reactor.

The major breakthrough for this technology will be the development and demonstration of a reactor capable of simultaneous synthesis and hydrolysis of zinc nanoparticles with the ability to recover the ZnO particles. We anticipate that operation at temperatures below Zn saturation and a rapid quench of the evaporated zinc will lead to improved particle yield. Significant improvement in the particle yield is needed for practical hydrolysis reactors in which the ZnO is recovered for thermolysis in a solar concentrating system.

Acknowledgment

The authors appreciate the encouragement of Professor Aldo Steinfeld at the ETH-Zurich to pursue this avenue of research and for the advice and helpful discussions as we began the study. The project is funded by the University of Minnesota Initiative for Renewable Energy and the Environment.

References

[1] Nakamura, T., 1977, "Hydrogen Production From Water Utilizing Solar Heat at High Temperatures," Sol. Energy, **19**(5), pp. 467–475.
[2] Steinfeld, A., Kuhn, P., Reller, A., Palumbo, R., Murry, J., and Tamaura, Y., 1998, "Solar-Processed Metals as Clean Energy Carriers and Water Splitters," Int. J. Hydrogen Energy, **23**, pp. 767–774.
[3] Fletcher, E. A., 2001, "Solarthermal Processing: A Review," ASME J. Sol. Energy Eng., **123**, pp. 63–74.
[4] Perkins, C., and Weimer, A. W., 2004, "Likely Near-Term Solar-Thermal Water Splitting Technologies," Int. J. Hydrogen Energy, **29**, pp. 1587–1599.
[5] Steinfeld, A., 2005, "Solar Thermochemical Production of Hydrogen—A Review," Sol. Energy, **78**, pp. 603–615.
[6] Abanades, S., Charvin, P., Flamant, G., and Neveu, P., 2006, "Screening of Water-Splitting Thermochemical Cycles Potentially Attractive for Hydrogen Production by Concentrated Solar Energy," Energy, **31**, pp. 2805–2822.
[7] Palumbo, R., Lédé, J., Boutin, O., Elorza, Ricart E., Steinfeld, A., Moeller, S., Weidenkaff, A., Fletcher, E. A., and Bielicki, J., 1998, "The Production of Zn From ZnO in a Single Step High Temperature Solar Decomposition Process," Chem. Eng. Sci., **53**, pp. 2503–2518.
[8] Haueter, P., Moeller, S., Palumbo, R., and Steinfeld, A., 1999, "The Production of Zinc by Thermal Dissociation of Zinc Oxide—Solar Chemical Reactor Design," Sol. Energy, **67**, pp. 161–167.
[9] Moeller, S., and Palumbo, R., 2001, "Solar Thermal Decomposition Kinetics of ZnO in the Temperature Range 1950–2400 K," Chem. Eng. Sci., **56**, pp. 4505–4515.
[10] Schunk, L. O., Haeberling, P., Wepf, S., Wuillemin, D., Meier, A., and Steinfeld, A., 2007, "A Rotary Receiver-Reactor for the Solar Thermal Dissociation of Zinc Oxide," *Proceedings of the ASME Energy Sustainability Conference*, Long Beach, CA, Jun. 27–30, Paper No. 36078.
[11] Perkins, C., Lichty, P., and Weimer, A. W., 2007, "Determination of Aerosol Kinetics of Thermal ZnO Dissociation by Thermogravimetry," Chem. Eng. Sci., **62**, pp. 5952–5962.
[12] Steinfeld, A., 2002, "Solar Hydrogen Production Via a Two-Step Water-Splitting Thermochemical Cycle Based on Zn/ZnO Redox Reactions," Int. J. Hydrogen Energy, **27**, pp. 611–619.
[13] Elorza-Ricart, E., Martin, P. Y., Ferrer, M., and Lédé, J., 1999, "Direct Thermal Splitting of ZnO Followed by a Quench. Experimental Measurements of Mass Balances," J. Phys. IV, **9**, pp. 325–330.
[14] Weidenkaff, A., Reller, A., Sibieude, F., Wokaun, A., and Steinfeld, A., 2000, "Experimental Investigations on the Crystallization of Zinc by Direct Irradiation of Zinc Oxide in a Solar Furnace," Chem. Mater., **12**, pp. 2175–2181.
[15] Ernst, F. O., 2007, "Co-Synthesis of H_2 and Nanocrystalline ZnO Particles by Zn Aerosol Formation and In Situ Hydrolysis," Ph.D. thesis No. 17272, ETH-Zurich, Zurich.
[16] Vishnevetsky, I., and Epstein, M., 2007, "Production of Hydrogen From Solar Zinc in Steam Atmosphere," Int. J. Hydrogen Energy, **32**(14), pp. 2791–2802.
[17] Berman, A., and Epstein, M., 2000, "The Kinetics of Hydrogen Production in the Oxidation of Liquid Zinc With Water Vapor," Int. J. Hydrogen Energy, **25**, pp. 957–967.
[18] Weidenkaff, A., Reller, A. W., Wokaun, A., and Steinfeld, A., 2000, "Thermogravimetric Analysis of the ZnO/Zn Water Splitting Cycle," Thermochim. Acta, **359**, pp. 69–75.
[19] Wagner, C., and Grunewald, K., 1936, "Beitrag zur Theorie des Anlaufvorgangs," Z. Phys. Chem. Abt. B, **40**(6), pp. 455–475.
[20] Park, K., Lee, D., Rai, A., Mukherjee, D., and Zachariah, M. R., 2005, "Size Resolved Kinetic Measurements of Aluminum Nanoparticle Oxidation With Single Particle Mass Spectrometry," J. Phys. Chem. B, **109**(15), pp. 7290–7299.
[21] Rai, A., Lee, D., Park, K. J., and Zachariah, M. R., 2004, "Importance of Phase Change of Aluminum in Oxidation of Aluminum Nanoparticles," J. Phys. Chem. B, **108**(39), pp. 14793–14795.
[22] Rai, A., and Zachariah, M. R., 2006, "Understanding the Mechanism of Aluminum Nanoparticle Oxidation," Combust. Theory Modell., **10**(5), pp. 843–859.

[23] Weiss, R. J., Ly, H. C., Wegner, K., Pratsinis, S. E., and Steinfeld, A., 2005, "H_2 Production by Zn Hydrolysis in Hot-Wall Aerosol Reactor," AIChE J., **51**, pp. 1966–1970.
[24] Wegner, A. K., Ly, H. C., Weiss, R. J., Pratsinis, S. E., and Steinfeld, A., 2006, "In Situ Formation and Hydrolysis of Zn Nanoparticles for H_2 Production by the 2-Step ZnO/Zn Water-Splitting Thermochemical Cycle," Int. J. Hydrogen Energy, **31** pp. 55–61
[25] Ernst, F. O., Tricoli, A., Pratsinis, S. E., and Steinfeld, A., 2006, "Co-Synthesis of H_2 and ZnO by In Situ Zn Aerosol Formation and Hydrolysis," AIChE J., **52**(9), pp. 3297–3303.
[26] Wang, S. C., and Flagen, R. C., 1990, "Scanning Electrical Mobility Spectrometer," Aerosol Sci. Technol., **13**, pp. 230–240.
[27] Yaws, C. L., 1999, *Chemical Properties Handbook*, McGraw-Hill, New York.
[28] Clarke, J. A., and Fray, D. J., 1979, "Oxidation of Zinc Vapour by Hydrogen-Water Vapor Mixtures," Trans. Inst. Min. Metall., Sect. C, **88**, pp. 161–166.